

DESIGN AND ANALYSIS FOR EXPERIMENTAL VALIDATION OF TOUCHLESS CHARGE CONTROL TESTING

James D. Walker III*, Julian Hammerl†, and Hanspeter Schaub‡

Unaccounted electrostatic forces during proximity operations between charged spacecraft introduce additional perturbations and can also lead to arcing and collisions. Geostationary and cislunar regions are becoming more popular, so the ability to measure the potential of a non-cooperative target spacecraft and account for these forces becomes more important. Proposed techniques for remotely sensing the electric potential of neighboring spacecraft utilize an electron beam emitted from a servicer, impacting the surface of the neighboring craft to excite secondary electrons and x-rays. Terrestrial experiments succeeded in measuring the steady state potential of a target object in a vacuum chamber; however, for a more realistic analysis of remote sensing techniques, the transient behavior of spacecraft charging must be examined. In this paper, an RC circuit and high voltage power supply are connected to the target object in order to simulate the response of a spacecraft to the plasma environment. A derivation is presented relating the resistance, capacitance and voltage of the circuit to the space environment, with the purpose of approximating different plasma regimes by tuning the parameters of the RC circuit. The emission of secondary and backscattered electrons from the target object complicates the experiments, but an estimate of the electron losses is found for the given experimental setup. The comparison of the discharging behavior of the circuit and the spacecraft charging model shows the RC circuit is representative of the space environment when the difference between the spacecraft potential and the natural potential is small.

INTRODUCTION

On-orbit servicing, assembly, and manufacturing activities (OSAM) have been identified as critical technologies for future mission concepts.¹ These operations often require two or more satellites performing proximity maneuvers and docking. Interactions between the charged plasma of the space environment and a spacecraft lead to electric charge accumulating on its surface. As two satellites approach each other, electrostatic forces and torques are generated between the two objects. These forces cause perturbations during proximity operations, decreasing the performance of relative motion controls and can even lead to collisions between the two craft if not accounted for.² Rendezvous operations can also lead to electrical arcing as satellites with different potentials approach each other for docking. A spacecraft with the ability to determine the electrical potential of a neighboring craft is able to use this knowledge during proximity and rendezvous operations.

*Graduate Research Assistant, Ann and H.J. Smead Department of Aerospace Engineering Sciences, University of Colorado Boulder, Colorado Center for Astrodynamics Research, Boulder, CO, 80303 USA. James.WalkerIii@colorado.edu

†Graduate Research Assistant, Ann and H.J. Smead Department of Aerospace Engineering Sciences, University of Colorado Boulder, Colorado Center for Astrodynamics Research, Boulder, CO, 80303 USA. julian.hammerl@colorado.edu

‡Professor and Department Chair, Schaden Leadership Chair, Ann and H.J. Smead Department of Aerospace Engineering Sciences, University of Colorado, Boulder, 431 UCB, Colorado Center for Astrodynamics Research, Boulder, CO, 80309. AAS Fellow, AIAA Fellow.

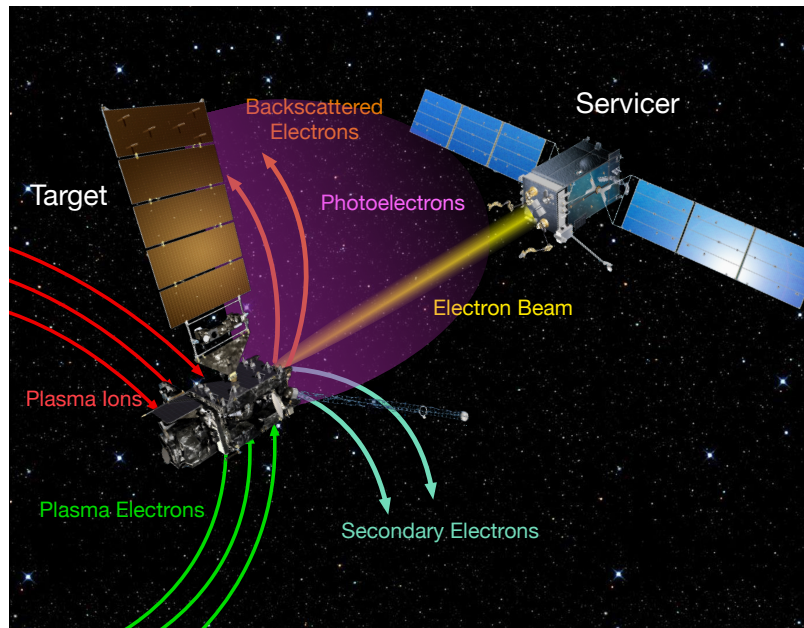


Figure 1. Conceptual representation of a satellite exposed to the space environment and an electron beam

With the electrical charge of the target object, a self measurement of electric charge, and the distance between them, the electrostatic forces and torques between two neighboring spacecraft can be calculated. When this is incorporated into the relative motion control of the spacecraft, these additional perturbations are accounted for, improving the performance of the controller and decreasing the possibility of a collision.² This is especially beneficial for docking operations because as the distance between two charges decrease, the Coulomb force between them increases exponentially and becomes a more significant perturbation. Spacecraft charging can also be caused by non-natural currents such as those caused by electron beams, ion beams, and ultraviolet lasers.³ For this paper, "charge control" refers to the use of one or more non-natural currents in order to alter the electrical potential on a neighboring spacecraft. An active charge control method that has been proposed for contactless electrostatic stabilization of a target is the Electrostatic Tractor.⁴ The goal is to apply an additional current to a target with the purpose of controlling the charges of a servicing craft and a target object. The Electrostatic Tractor utilizes a high energy electron gun attached to a servicing spacecraft. When activated, a beam of electrons induces a negative current on a target object; however, because electrons are being emitted by the servicer, the servicing craft tends to charge positively.^{4,5} These charges generate an electrostatic force between the two satellites which is then utilized for the electrostatic maneuvers.¹ The Electrostatic Tractor (ET) has been proposed as a contactless method of large debris removal.^{4,5} By utilizing the forces and torques caused by spacecraft charging, the servicing craft can stabilize the debris and then move it to a graveyard orbit.^{4,5} Reference 6 found that estimation errors of the electric potential of the debris can significantly affect the bounds of safe operation of the ET relative motion control, suggesting that the Electrostatic Tractor would benefit from remote electric potential sensing methods.

The ability to remotely sense the electric potential of a neighboring spacecraft improves relative motion control efficiency of proximity and docking maneuvers and is required for charge control techniques such as the Electrostatic Tractor. Two methods that have been explored utilize a positively charged servicing spacecraft equipped with a high energy electron beam to excite secondary

electrons and x-rays from a target object.^{5,7} The secondary electrons are attracted toward the servicing craft and impact with an energy equal to the difference in electric potential between the two objects while the emitted x-rays have an energy equal to the energy difference of target object and electron beam; therefore, comparing the measured x-ray energies and the electron beam energy yields the electric potential of the target.^{5,7} To measure its own potential, the spacecraft is equipped with a langmuir probe. These instruments have been proposed for use on spacecraft for measuring plasma density and electron temperature together with the spacecraft potential.⁸ The servicing craft measures the energy spectrum of the electrons (or the photons depending on which method is being employed) and knowing its own potential, determines the potential of the target object.

Both methods have been experimentally validated for vacuum chamber conditions^{9,10} in the Electrostatic Charging Laboratory for Interactions between Plasma and Spacecraft (ECLIPS) research vacuum chamber.¹¹ An electron beam is used to excite secondary electrons and x-rays from a small, usually aluminum, object used to represent a spacecraft. An x-ray detector is used to measure the energies of emitted x-ray photons while a Retarding Potential Analyser (RPA) measures the flux and energy of the secondary electrons.¹¹ The RPA is similar to a gridded Faraday cup where electrons with energy less than or equal to the potential across the grid can not pass through.¹¹ When sweeping through the energy spectrum, the grid potential that corresponds to a large drop off in current indicates the potential difference between the electron gun and the target. The experiments were conducted using a high voltage power supply (HVPS) to control the potential of the target object. While this is useful to test and validate remote sensing methods, the charge of a spacecraft is not always constant. Additionally, an electron beam applies a current to the target. Because the HVPS maintains a constant potential on the target, the charging effect due to the electron beam is eliminated.

In order to explore remote sensing methods in a more realistic capacity and conduct charge control experiments, the potential of the target object must be allowed to fluctuate with the electron beam current during experiments. To achieve this, it is proposed that an external circuit is connected to the testing object outside the vacuum chamber. There are three goals of this circuit: increase the capacitance of the target object to allow the charging behavior to be measured, create charging behavior similar to that caused by the space environment, and simulate the natural potential of an object while still allowing the electron gun to alter the charge of the target. It was determined that a parallel RC circuit with an HVPS was best to achieve this. This paper includes an overview of the spacecraft charging model and experimental setup, the derivation of the relationship between the charging model and the RC circuit, and the experimental results.

MATERIALS AND METHODS

Spacecraft Charging Model

Solar wind consists of electrons and ions flowing through space and the difference in the ambient flux of these particles causes charging.¹² Due to the mass difference, electrons are much faster than ions, leading to a significantly larger electron flux impacting the surface of a spacecraft. The ambient ions apply a positive current on the object, however it is typically less than the negative current of the ambient electrons.¹² Other natural currents experienced by a satellite include photoelectron current from the Sun, current from secondary electron emissions (SEE), and current from backscattered electrons.¹² The sunlit side of a spacecraft is exposed to the high energy photons produced by the Sun. Surface electrons are excited by these impacting photons and are emitted from the craft if it is charged negatively.¹² The secondary electron current is caused by low energy electrons removing

electrons from the surface of an object.¹² These impacting, also known as "primary", electrons transfer some of their energy to the surface electrons. If enough energy is shared, one or more secondary electrons are emitted from the spacecraft. Sometimes, instead of being absorbed by the target, a primary electron is reflected off the surface, generating a backscattered electron.¹² Unlike secondary electrons, only one backscattered electron can be produced by a primary electron.

These currents are driven by the plasma density, the lighting conditions, and energy of impacting electrons, all of which vary between regions of space. When in sunlight, spacecraft typically charge weakly positive due to the dominating photoelectric current while objects in eclipsed geostationary orbits can charge to a few kilo-volts negative because of ambient electron current.¹² The equilibrium of these currents determines the natural potential of an object as well as the transient behavior of the charging. An electron beam generates an additional current: a positive current on the spacecraft emitting the electrons and a negative current on the target object.

This paper utilizes a charging model that simulates the natural currents experienced by an object in different regions of space as well as an electron beam current. It assumes a conducting spacecraft with spherical geometry. A model for secondary electrons and backscattered electrons is presented here, but in order to achieve a time invariant result, it is not considered for the design of the circuit, but only for running numerical spacecraft charging simulations. While not all spacecraft satisfy these conditions the following is a simplified approach for comparing the space environment to an RC circuit.

The plasma electron current is

$$I_e(\phi) = -\frac{Aqn_e\omega_e}{4}e^{\phi/T_e} \quad \phi < 0 \quad (1a)$$

$$I_e(\phi) = -\frac{Aqn_e\omega_e}{4}\left(1 + \frac{\phi}{T_e}\right) \quad \phi \geq 0, \quad (1b)$$

where n_e , T_e , and m_e are the electron density, temperature, and mass respectively, ϕ is the spacecraft potential, A is the surface area exposed to the plasma, q is the elementary charge, and $\omega_e = \sqrt{8T_e/\pi m_e}$ is the thermal velocity of electrons.¹³

Similarly, the plasma ion current is

$$I_i(\phi) = \frac{Aqn_i\omega_i}{4}e^{-\phi/T_i} \quad \phi > 0 \quad (2a)$$

$$I_i(\phi) = \frac{Aqn_i\omega_i}{4}\left(1 - \frac{\phi}{T_i}\right) \quad \phi \leq 0. \quad (2b)$$

The variables are defined the same as in Eq. (1) except the subscript i denotes ions.¹³ An ion flux consisting of solely protons is assumed here.

When a spacecraft is in sunlight, high energy photons excite electrons away from the spacecraft generating a photoelectron current. For negatively charged spacecraft, the electrons are repelled away from the object. For positively charged spacecraft, the low energy electrons are recaptured by the spacecraft. Once an object charges positive due to the photoelectron current, it will only remain weakly positive. This photoelectron current is

$$I_{ph}(\phi) = j_{ph,0}A_{\perp}e^{-\phi/T_{ph}} \quad \phi > 0 \quad (3a)$$

$$I_{ph}(\phi) = j_{ph,0}A_{\perp} \quad \phi \leq 0, \quad (3b)$$

with, A_{\perp} being the cross-sectional area exposed to the sunlight, $T_{ph} = 2$ eV being the temperature of emitted photoelectrons, and the photoelectron flux is assumed to be $j_{ph,0} = 20 \mu\text{A}/\text{m}^2$.¹²

When active, the electron beam applies a negative current on the target object. This current only occurs while the difference in electric potential between the servicer and the target is less than the initial energy E_{EB} of the electron beam. When the difference is greater than or equal the electron beam energy, the emitted electrons do not have enough energy to reach the target. This current is expressed by

$$I_T(\phi_T) = -\alpha I_{EB} \quad \phi_S - \phi_T < E_{EB} \quad (4a)$$

$$I_T(\phi_T) = 0 \quad \phi_S - \phi_T \geq E_{EB}, \quad (4b)$$

where ϕ_S and ϕ_T are the potentials of the servicer and target respectively, I_{EB} is the current of the electron beam and α is the fraction of the beam hitting the target. A value of $\alpha = 1$ is used, assuming an accurate and focused beam so $I_T = -I_{EB}$ if the beam reaches the target.

Impacting low energy electrons and ions can cause the emission of secondary and backscattered electrons.¹² These electrons are repelled away from a negatively charged target and can cause a significant positive current on the target. Reference 14 surveys various secondary electron emission models for spacecraft and demonstrates that different models yield significantly different results. The approximation developed in Ref. 15 where

$$I_{SEEB}(\phi_T) = -4Y_{\max}I_T(\phi)\kappa \quad \phi < 0 \quad (5a)$$

$$I_{SEEB}(\phi_T) = 0 \quad \phi \geq 0, \quad (5b)$$

with

$$\kappa = \frac{E_{\text{eff}}/E_{\max}}{(1 + E_{\text{eff}}/E_{\max})^2} \quad (6)$$

and

$$E_{\text{eff}} = E_{EB} - \phi_S + \phi_T \quad (7)$$

is used because it allows for a simple analytic expression of I_{SEEB} , with, E_{eff} being the effective energy of the beam electrons when they impact the target, Y_{\max} being the maximum yield of electron emissions, and E_{\max} being the landing energy at which the maximum yield occurs. As established by Ref. 4, the material properties for aluminum, $Y_{\max} = 2$ and $E_{\max} = 300$ eV, are used. The value for Y_{\max} includes both secondary and backscattered electrons. At energies greater than 1 keV, the yield can become negligible.¹² These material properties are for pure, clean aluminum; however the surfaces of metals can oxidize over time. A comparison of different aluminum secondary electron yield (SEY) data sets is conducted in Ref. 16. The average SEY for clean aluminum was 1.43 while the average yield for aluminum oxide was 2.83, suggesting that a coating of aluminum oxide can double the secondary electron yield.¹⁶

These equations are used to represent the space environment; moreover, the natural potential occurs when the sum of the natural currents is zero

$$I_N(\phi_N) = I_{ph}(\phi_N) + I_i(\phi_N) + I_e(\phi_N) = 0. \quad (8)$$

The plasma density and temperature, driving factors of the ion and electron currents, differ significantly even in the same region of space: in geostationary orbits, plasma densities range from 0.1 - 1 cm^3 .¹² Different plasma currents are induced by the differing plasma properties. In eclipsed

regions, there is no photoelectron current and the plasma determines the natural potential. However, in sunlight regions, the photoelectron emission often dominates spacecraft charging.¹² This means a satellite that orbits in and out of eclipse can charge between a few kilo-volts negative to a few volts positive within the span of one orbit. The electron beam applies additional currents, altering

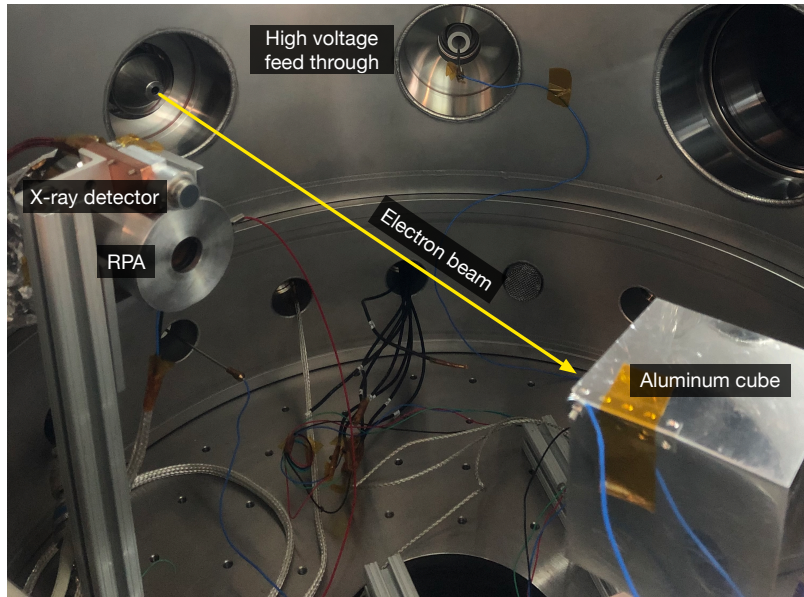


Figure 2. The experimental setup inside the ECLIPS vacuum chamber with a cube as the target object¹¹

the potential of the spacecraft such that

$$I_{\text{tot}}(\phi) = I_{EB} + I_{SEE}(\phi) + I_{ph}(\phi) + I_i(\phi) + I_e(\phi). \quad (9)$$

When the electron beam is turned off, the spacecraft returns to the natural potential. The ambient currents determine this behaviour as well; they can be used to model how the spacecraft will lose the extra charge.

Experimental Setup

Experiments are conducted in the ECLIPS vacuum chamber with an experimental setup shown in Fig. 2.¹¹ The experimental setup consists of a high energy electron gun, a 70 x 70 x 70 mm aluminum cube used to simulate the bus of a spacecraft, the RPA, and an additional RC circuit. The electron gun is a EMG-4212C from Kimball Physics. It is capable of emitting electrons with currents ranging from 0.1 μA to 100 μA and with energies ranging from 0.1 keV to 30 keV. Before experiments are conducted, the impact location of the beam is verified using a 38 mm diameter Kimball Physics Rugged Phosphor Screen. Blue light is emitted when electrons impact the screen, which is used to center the beam.

Connected to the spacecraft model by a high voltage feed-through, the circuit is located outside the vacuum chamber. A diagram of the RC (resistor and capacitor) circuit used here as shown by Fig. 3 and Fig. 4 shows a picture of the actual circuit. The resistor and capacitor are connected in parallel underneath the board by high voltage wires. The copper strips of the board could not be connected to the components because they are close together and, at high voltages, arcing can

occur between them. In Fig. 4, the circuit is connected to the high voltage feed through and the ground. The red and black wires are the input and output, respectively, of the multimeter. When

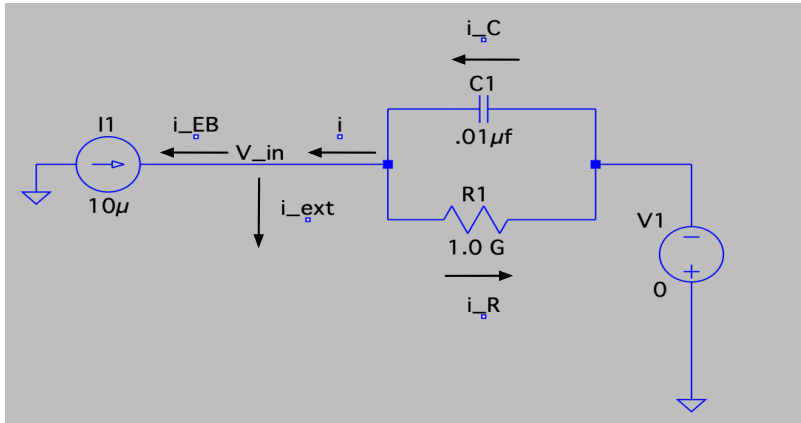


Figure 3. A schematic representative of the additional circuit connected to the target object

the electron beam is on, the cube charges quickly and current flows from the cube into the capacitor and through the resistor. When the beam is turned off, the capacitor discharges until it reaches the potential maintained by the voltage source, simulating the natural potential. While charging still occurs without the extra capacitor, the cube charges and discharges faster than the instruments can measure. Increasing the capacitance extends the charging process, simulating the behavior of large spacecraft and allowing the charging behavior to be measured. The charging rate is also affected by the size of the resistor; however, the maximum voltage the capacitor can reach is controlled by the resistor. The circuit is designed for the resistor and capacitor to be easily swapped out with components of varying sizes, allowing different charging behaviors to be generated. Resistance values range from 100 MΩ to 1 GΩ while capacitance values vary from 100 pF to .01 μF.

A Keithley Model DMM6500 6.5-Digit Multimeter is used as an amp-meter in series with the resistor and is capable of measuring currents as low as 10 pA. Although the voltage across the capacitor is the desired measurement, current through resistor is being measured. This is because the internal resistance of the multimeter is 10 MΩ, an order of magnitude less than the smallest resistor being used. Current flows through the path with the least resistance, therefore, when measuring voltage, it flows through the multimeter and we are not be able to change the charging behavior for a given capacitor. Instead, current through the resistor is being measured, and using Ohm's law ($I = \phi/R$), the voltage across the resistor is calculated. Components in parallel have the same voltage, so this is also the voltage across the capacitor.

The discharging behavior of the circuit is measured by using an HVPS to apply a voltage to the system and then disconnecting it, allowing the capacitor to discharge. A Matsusada AU-30R1 High-Voltage Power Supply is used to provide high quality potentials up to 30 kV with a maximum current of 1.0 mA.

Space Environment as an RC circuit

In order to develop an experimental setup that replicates the charging behavior of objects in space, one needs to determine the relationship between the RC circuit and the spacecraft charging model. This can be found by deriving the differential equation for voltage ϕ from the charging model and from the experimental setup in the ECLIPS vacuum chamber, then relating the two resulting

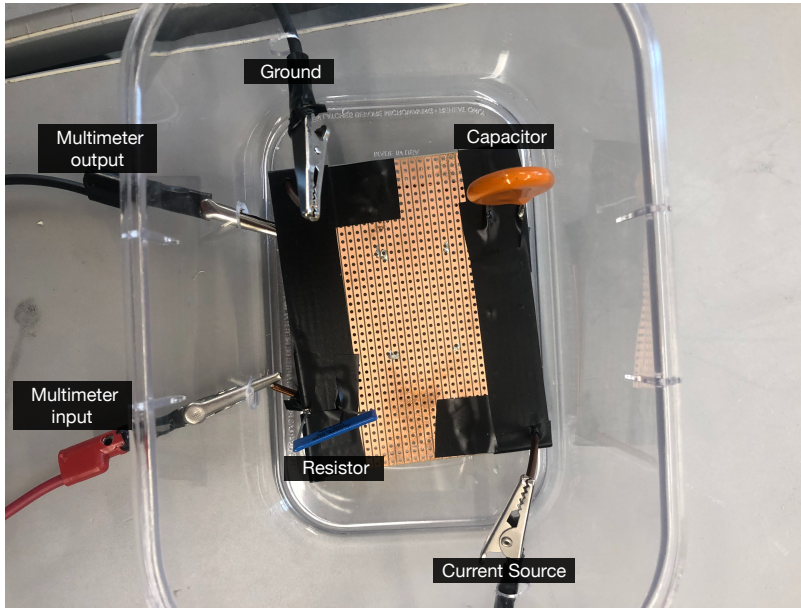


Figure 4. The RC circuit used in the experimental setup.

equations to obtain expressions for the capacitance C , resistance R , and floating potential ϕ_N as a function of the plasma and spacecraft properties.

When exposed to the space environment, the surface of the spacecraft charges based on the capacitance of the craft.¹² Because of this, an object in space can be simply modeled as a capacitor exposed to the same currents as the object. By reducing the problem to a capacitor and total current, the voltage of a spacecraft is described by

$$C_{SC} \frac{d\phi}{dt} = I_{\text{tot}}, \quad (10)$$

where C_{SC} is the capacitance of the spacecraft and I_{tot} is the instantaneous total current. With the total current being given by Eq. (9), a relationship between C_{SC} and ϕ can be found. The current experienced by a spacecraft depends on its potential as shown by the charging model. Equation (11) shows the derivation for an object with a negative potential, but it is similar for positively charged objects

$$C_{SC} \frac{d\phi}{dt} = -\frac{Aqn_e\omega_e}{4} e^{\phi/T_e} + \frac{Aqn_i\omega_i}{4} \left(1 + \frac{\phi}{T_i}\right) + j_{ph,0}A_{\perp} + I_{EB} + I_{SEEB}. \quad (11)$$

The electron beam utilizes high energy electrons, resulting in a low secondary (and backscattered) electron yield (SEY). At lower energies, around 300 eV, the SEY of aluminum has a significant contribution to the overall potential.¹² Also, as shown by Eq. (5), the secondary electron current varies with potential of the target object. Incorporating this current into the experimental setup up requires rapid and precise voltage measurements and, for the RC circuit to be related to the spacecraft charging model with the SEE, a time varying resistance would be required. The current caused by the secondary electron emission is small relative to other currents and because it allows an analytical expression for resistance to be simplified, the secondary electron current is not included.

In order to properly develop this relationship, I_e is linearized about the natural potential ϕ_N .

Using a first order Taylor expansion for e^{ϕ/T_e} , one gets

$$e^{\phi/T_e} = e^{\phi_N/T_e} + \frac{e^{\phi_N/T_e}}{T_e}(\phi - \phi_N) + H.O.T. \quad (12)$$

Therefore, the current due to ambient plasma electrons is approximately

$$I_e \approx -\frac{Aqn_e\omega_e}{4}e^{\phi_N/T_e}\left(1 + \frac{\phi}{T_e} - \frac{\phi_N}{T_e}\right). \quad (13)$$

While the potential is close to ϕ_N , the higher order terms are small, therefore they are not considered. If the difference between ϕ and ϕ_N is large, the higher order terms are significant and must be considered. Using this expression for the electron current and solving for the differential equation for ϕ , we get

$$C_{SC} \frac{d\phi}{dt} + \left(\frac{Aqn_i\omega_i}{4T_i} + \frac{Aqn_e\omega_e}{4T_e}e^{\phi_N/T_e}\right)\phi = \frac{Aqn_i\omega_i}{4} + j_{ph,0}A_{\perp} - \frac{Aqn_e\omega_e}{4}e^{\phi_N/T_e}\left(1 - \frac{\phi_N}{T_e}\right) + I_{EB}. \quad (14)$$

Note that the left-hand side of the equation is linear in ϕ and the right-hand side is constant. The next step is to determine the differential equation describing voltage from the circuit using Kirchhoff's Current Law around the V_{in} node. By balancing the currents into the node with the currents out of the node, the resulting relationship is

$$i_{ext} = i - i_{EB} = i_C - i_R - i_{EB} = C \frac{d\phi}{dt} - \frac{\phi_{N,RC} - \phi}{R} - i_{EB}, \quad (15)$$

with i_C being the current discharged by a capacitor and i_R being the current from the resistor given by Ohm's Law. Here, i is the current discharging from the cube and i_{ext} is an additional controlled current applied to the target that can simulate currents such as the photoelectron current or ion beam emission. The simulated natural potential of the circuit, $\phi_{N,RC}$ is controlled by the HVPS to match the natural potential of the charging model, ϕ_N . Reorganizing terms results in an equation with a similar form as Eq. (14).

$$C \frac{d\phi}{dt} + \frac{1}{R}\phi = \frac{\phi_{N,RC}}{R} + i_{ext} + i_{EB} \quad (16)$$

Both Eq. (14) and Eq. (16) describe the change in potential across the capacitor. By comparing the coefficients of the equations, a relationship between the space environment and the components of the circuit can be found as

$$C = C_{SC}, \quad (17)$$

$$R = \frac{1}{\frac{Aqn_i\omega_i}{4T_i} + \frac{Aqn_e\omega_e}{4T_e}e^{\phi_N/T_e}}, \quad (18)$$

and

$$i_{ext} = \frac{Aqn_i\omega_i}{4} + j_{ph,0}A_{\perp} - \frac{Aqn_e\omega_e}{4}e^{\phi_N/T_e}\left(1 - \frac{\phi_N}{T_e}\right) - \frac{\phi_N}{R}. \quad (19)$$

These equations allow for the space environment to be represented by the circuit. The spacecraft capacitance is simply equal to the value of the circuit capacitor. Resistance and the external current, on the other hand, depend on the space weather conditions such as electron and ion density, ion temperature, and floating potential. The value for ϕ_N is determined numerically by finding the root of Eq. (8). With ϕ_N , the resistance R and external current I_{ext} can be found as well by solving

Eq. (18) and (19) respectively. For these experiments, there is no external current being applied so $i_{\text{ext}} = 0$.

Other circuit models for have been developed for the purpose of spacecraft charging. Reference 17 models the ambient plasma in terms of a Maxwellian distribution function, but does not model an electron beam. Also, numerical methods are used to compute the capacitance of conducting objects in free space.¹⁷

The next section uses experiments in the ECLIPS vacuum chamber to validate the relationship derived here.

RESULTS

Charging of a Free Floating Target

In order to demonstrate that the electron gun is capable of charging a target object in the ECLIPS vacuum chamber, the cube is disconnected from the high voltage feed through, simulating a 'floating' object. Because the cube is disconnected from the high voltage feed through, the potential on the object cannot be measured using the multimeter. Instead, the secondary electron method is employed to determine the potential of the object. This remote electric potential sensing technique has been investigated extensively in Refs. 10, 18, 19.

Figure 5 shows the spectrum of electrons that the cube emits at an angle of 18 degrees, measured by a Retarding Potential Analyzer (RPA, see Refs. 10, 11). The zero angle is defined as the orientation of the cube where the front cube face is perpendicular to the electron gun. Because the surface of the cube is not perfectly smooth and not all the secondary electrons are being detected, the RPA only measures a relative current from the secondary electrons and not the actual SEE shown by Eq. (5). Conclusions about the SEE can not be drawn from this experiment, but it can be used to determine the potential of the target The electron beam current is kept constant at $10 \mu\text{A}$ and the

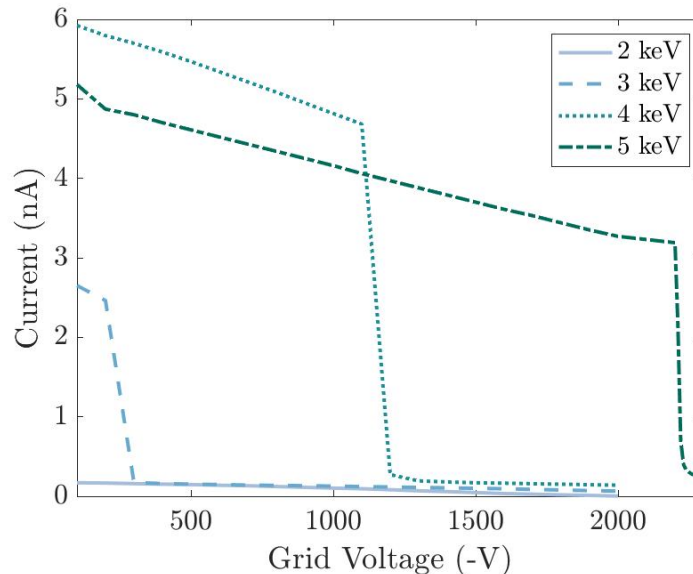


Figure 5. Spectrum of electrons emitted from the cube taken with the RPA located at an angle of 18 deg.

energy is varied between 2 keV and 5 keV. While beam energies up to 5 keV are being used, the spectrum of electrons being measured is only up to 2.3 keV. Because this is a rudimentary, in-house RPA, high voltage differences can lead to electric arcing across the grid. For energies between 2-4 keV, the grid voltage is not raised above 2 kV to ensure accurate measurements. For a 5 keV beam energy, the target charges to a potential greater than 2 kV, therefore the grid voltage is raised to 2.3kV and arcing between the grid was not observed.

Using the 2 keV beam energy, only noise was recorded across all grid voltages. This indicates that with a centered, focused beam of 2 keV, the target object does not charge in the vacuum chamber. For 3 - 5 keV, the current decreases linearly until it suddenly drops. This sudden drop corresponds to the potential of the object. For a 3 keV electron beam, the target charges to about -280 V while for the 4 keV beam, the target charges to -1.22 kV. The 5 keV beam charges the target to -2.21 kV. The only known current acting on the cube is the electron beam. For a 3 keV beam energy, one expects the cube to charge until it reaches -3 kV because electrons with an initial energy of 3 keV are not energetic enough to reach the cube if it is charged to more than 3 kV. However, for all beam energies, the measured potential of the cube is lower than the expected potential, suggesting some unknown positive current. This is likely caused by the secondary electron emissions.

In Ch. 9 of Ref. 12, it is explained that the behavior of electron beam charging depends on the impact energy of electron beam electrons.¹² Secondary electrons are generated when an electron impacts with an energy E . If the primary electron impact energy falls between the crossover energies E_1 and E_2 , it is probable that for each primary electron impact, there is more than one secondary electron emitted.¹² This generates a positive current on the target, therefore the target charges differently depending on the impact energy.¹² Figure 6 describes the surface charging behavior of electron beam impacts. Each circle represents a different set of initial target potentials and impact energy. The arrow indicates the charging behavior of the scenario while the end indicates the final target potential. Each arrow is drawn with an angle of ± 45 degrees with respect to the horizontal in order to show that, regardless of the initial conditions, the resulting behavior is linear with a slope of 1. The initial potential of the target is 0 V in each experiment, regardless of beam energy. When the impact energy is within the range of E_1 and E_2 , the outgoing secondary electron current is greater than the incoming electron current. Because of this, the target charges slightly positive, but, now that there is a positive charge, the removed electrons are attracted back to the target. This means the charge of the target remains close to 0 V. If the impact energy is greater than E_2 , the target charges negatively, until the impact energy reaches E_2 . Figure 6 demonstrates that with a negative target potential, E_2 is a stable equilibrium; therefore, once the impact energy reaches this point, it remains at this energy.

The impact energy is the difference between the beam energy and the target potential. For a 3 keV beam energy, the target charges to -280 V, indicating an impact energy of 2.72 keV. A 4 keV beam impacts on a target charged to -1.22 kV with an impact energy of 2.78 keV, and a 5 keV beam energy has an impact energy of 2.79 keV for a target with a potential of -2.21 kV. The impact energy decreases until it reaches an average energy of 2.76 keV, suggesting that $E_2 \approx 2.76$ keV. This is also supported by that fact that for a 2 keV beam energy, the resulting target potential is 0 keV. This beam energy is in the range where the secondary electron flux is greater than that of the electron beam, and because the starting potential is 0 kV, the target does not charge. Additionally, increasing the beam energy by 1 keV (and therefore the initial primary electron impact energy), decreases the target potential by approximately the same amount, a relationship that is consistent with Fig 6. In Ref. 20, a theoretical secondary electron curve for relativistic electrons impacting an aluminum

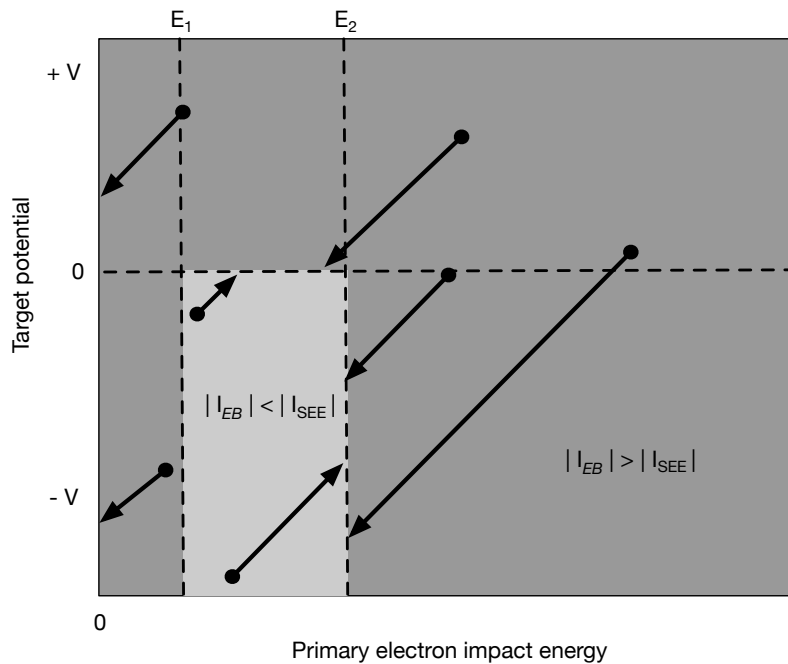


Figure 6. The surface charging of electron beam impacts. Each arrow represents the behavior of a spacecraft charged to a certain potential being impacted by a beam of a certain energy. Adapted from Ref. 12.

oxide surface is derived. This yield curve suggests that the value for E_2 is 2.2 keV²⁰ for aluminum oxide. Secondary electron yield curves vary between data sets; the general curve is similar but the energy and yield values vary.¹⁶ This is due to multiple factors including differences in material properties, target geometry and surface roughness. The thickness of the oxidized layer also affects the SEY behavior: a 3 nm layer has a larger SEY than that of a 1 nm layer.²¹ The measured value for E_2 in this experiment is similar to the value estimated in Ref. 20 and the difference in the values is due to differences and uncertainties for SEE models and experiments. This suggests that there is a layer of aluminum oxide on the target object and the secondary and backscattered electrons are the cause of the unexpected charging behavior. Note that the value for E_2 found in this work does not correspond to the E_2 value of a secondary electron yield curve, as it also includes backscattered electrons, self-emitted electrons due to the high potential, and other unknown losses. Instead, the value for E_2 found here provides an estimate for the losses of electrons, and can be accounted for in future work to characterize the experimental setup.

Discharging Behavior

To explore the discharging behavior, the circuit is disconnected from the cube and attached to an HVPS. The initial voltage across the capacitor must be known in order to compare the experiments to the spacecraft charging model and, while the electron beam does charge the object, the control of the voltage is much less precise. The capacitance of the cube is negligible, therefore removing it from the system does not have a significant effect on the results. The HVPS charges the circuit instantly and is then disconnected from the circuit. If the power supply is simply turned off (not disconnected), the capacitor will discharge through the power supply because its internal resistance is less than that of the resistors being used. Once the HVPS is removed, the current through the resistor is measured. The power supply in the circuit that allows the natural potential to be controlled

is not connected for these experiments, meaning the simulated natural potential is 0 V. The spectrum

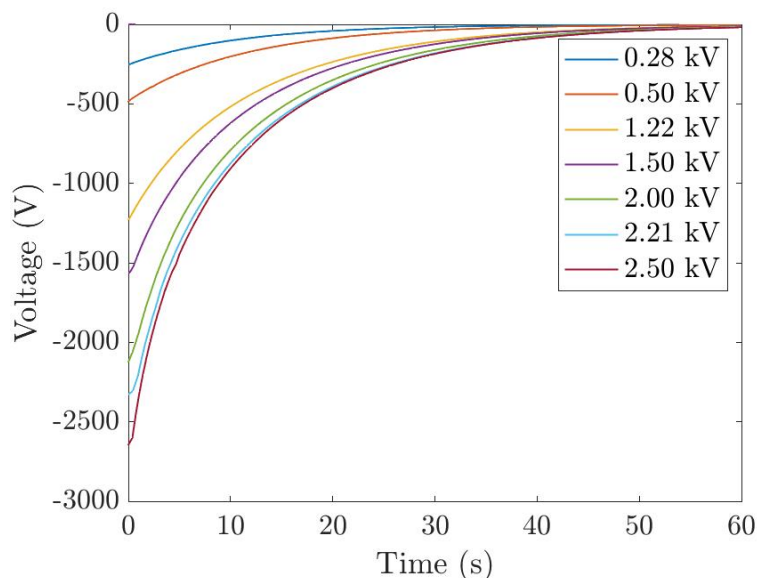


Figure 7. The discharging behavior of the RC circuit at starting voltages ranging from -280 V to -2.5 kV

of voltages being applied ranges from -280 V to -2.50 kV. For each starting voltage, the initial value is slightly different from the applied voltage. This is due to inaccuracies in the HVPS and the actual applied voltage has an error of about $\pm 5\%$ which must be considered when comparing these behaviors to the spacecraft charging model. One of the goals of the additional circuit is to increase the time it takes for the voltage across the capacitor to decrease in order to allow measurements to be taken. As shown by Fig 7, even for -280 V, it takes about 35 seconds for the voltage to increase above -10 V. This is sufficient time to measure the transient charging behavior of the target object.

In order to have a meaningful comparison between the discharging experiments and the spacecraft charging model, Eqs. (17-19) are used to find space environment parameters that result in an equivalent resistance of 1 G Ω and $\phi_N = 0$. An environment consisting of $T_i = 8.1$ keV, $T_e = 600$ eV, $n_i = 0.7896$ $1/\text{cm}^3$, and $n_e = 0.06766$ $1/\text{cm}^3$ results in a resistance value of $R = 1$ G Ω and $\phi_N = 0.388$ V. While the natural potential is not exactly 0, it is close enough to allow for a meaningful comparison. Figure 8 shows the comparison between discharging behavior for the spacecraft charging model and the RC circuit at low voltages of -280 V and -500 V. Because of the inherent $\pm 5\%$ error of the HVPS, the actual starting potentials are -235.2 V and -484.4 V respectively. Similarly, Fig. 9 shows this comparison for higher voltages of -1.5 kV and -2.0 kV. Likewise, the actual potential values are -1.562 kV and -2.124 kV respectively. As shown by Fig. 8, for low voltages, the two scenarios have nearly identical discharging behavior. There are some slight deviations, but for -253.2 V and -484.4 V, the RC circuit is a relatively accurate approximation for the space environment. According to Fig. 9, when the potential is larger, the approximation is no longer as accurate. With a -1.562 kV potential, there is greater than a 300 V difference between the two models at certain times. For a potential of -2.124 kV, this difference can be greater than 600 V. These inconsistencies can be explained by the approximations made during the derivation of Eqs. (17-19). A first order Taylor series expansion about the natural potential ϕ_N was used to linearize the ambient electron current I_e and the higher order terms were considered negligible. This as-

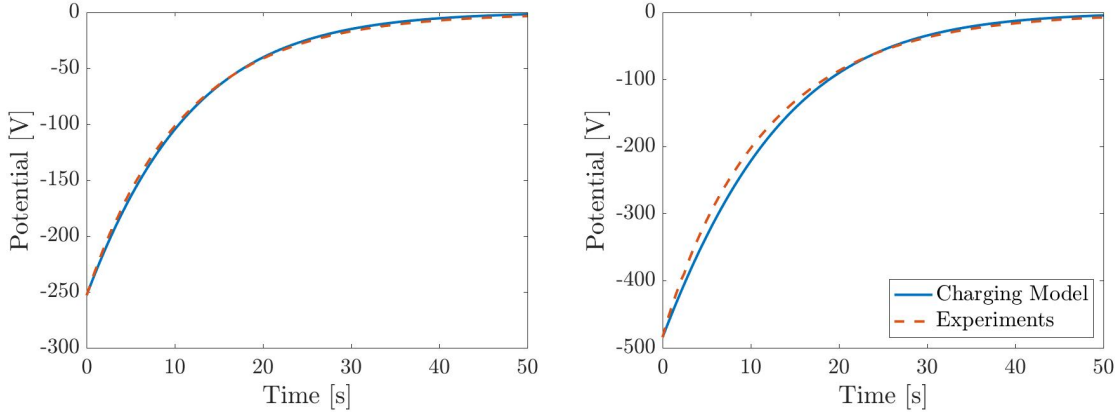


Figure 8. A comparison of the discharging behavior between the spacecraft charging model and the RC circuit for low starting voltages of (Left) -253.2 V and (Right) -484.4 V

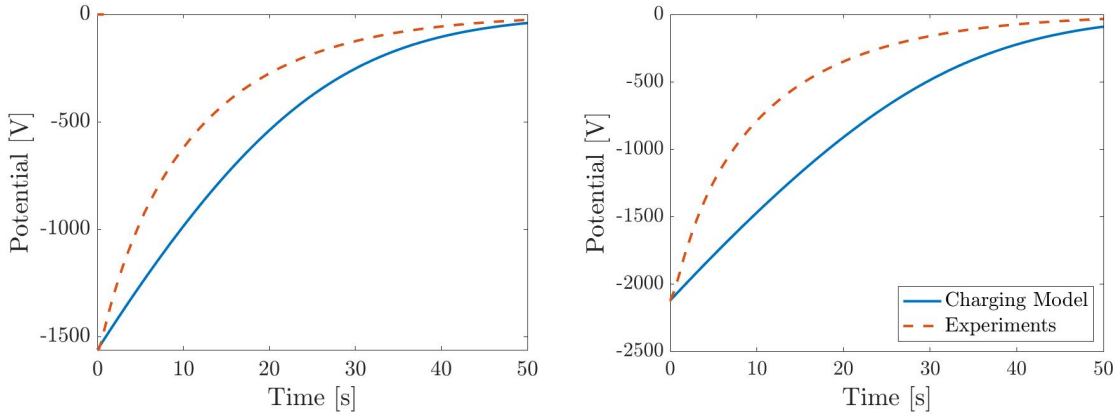


Figure 9. A comparison of the discharging behavior between the spacecraft charging model and the RC circuit for high starting voltages of (Left) -1.562 kV and (Right) -2.124 kV

sumption only holds if the difference between the spacecraft potential ϕ and ϕ_N is small. For these experiments, $\phi_N = 0$, so the lower voltages of -253.2 V and -484.4 keep this difference small and the higher order terms only cause minor differences between the two models. However, when higher voltages are used, this difference becomes large and the higher order terms have a significant effect on the resulting resistance value.

The goal of remote sensing methods is to measure the potential of a target, typically the floating potential. During sensing, the electron beam alters this potential, resulting in measurements where $\phi \neq \phi_N$. In order to yield reliable results, these sensing methods must keep the difference between ϕ and ϕ_N small, meaning for these methods, this model would accurately simulate the charging behavior. On the other hand, electrostatic detumbling often causes a spacecraft to deviate significantly from the natural potential.⁵ A scenario in a nominal GEO space weather conditions is explored in Ref. 5 where the natural potential is -3.21 keV; however, for this charging scenario, the target reaches a potential of -15.3 kV.⁵ Because of these large differences between ϕ and ϕ_N , this would not be accurate for electrostatic tractor methods; the high order terms of the Taylor expansion must be considered.

CONCLUSIONS

This work explores the ability to charge an aluminum target object to a non-zero potential using an electron beam and relates the response to a spacecraft charging model. The behavior of both charging and discharging of the target object is investigated. An RC circuit is added to increase the overall capacitance of the target and allow this behavior to be measured as well as to control the discharge current of the system.

By using a remote electric potential sensing method based on secondary electrons, the potential of a floating spacecraft shape primitive can be measured. The results demonstrate that the object can be charged using the electron beam, but to a lower potential than expected. This is caused by the secondary electron emissions driving the primary electron impact energy to a stable equilibrium value at the second crossover point of the SEY curve. Experiments designed to measure the discharge of the RC circuit show that the addition of the circuit extends the transient behavior of the system, allowing for measurements to be taken. Also, the comparison between the discharge of the RC circuit to that of the spacecraft charging model is used to support the use of the RC circuit to simulate the space environment at low voltages. At higher voltages, the approximations made in the derivation of the simplified theoretical framework no longer hold and the circuit is not an accurate representation of the space environment.

A key assumption throughout this paper is that the secondary electron yield is negligible at high energy impacting electrons. The floating potential experiments revealed that even at beam energies greater than 4 keV, the secondary electron emission (SEE) has a significant effect on the potential of the target. This is due to the contamination of the surface by aluminum oxide, which changes the material properties of the target. Before the charging behavior of the circuit can be compared to the charging model, the emission of secondary and backscattered electrons must be modeled and accounted for or a pure aluminum target must be used to ensure the material properties are correct. Once the charging behavior of the circuit is validated against the charging model, this experimental setup can be used to conduct charge control experiments, and the effect of the electron beam on remote sensing techniques can be explored.

ACKNOWLEDGMENTS

The authors would like to thank Dr. Álvaro Romero-Calvo for fruitful discussions on floating potential experiments. This work was supported by the U.S. Air Force Office of Scientific Research under grant FA9550-20-1-0025.

REFERENCES

- [1] H. Schaub and D. F. Moorer, “Geosynchronous Large Debris Reorbiter: Challenges and Prospects,” *The Journal of the Astronautical Sciences*, Vol. 59, Jun. 2012, pp. 161–176, 10.1007/s40295-013-0011-8.
- [2] K. Wilson, A. Romero-Calvo, and H. Schaub, “Constrained Guidance for Spacecraft Proximity Operations Under Electrostatic Perturbations,” *Journal of Spacecraft and Rockets*, 2022, pp. 1–13. in press, 10.2514/1.A35162.
- [3] A. Romero Calvo, K. Champion, and H. Schaub, “Touchless Spacecraft Potential Sensing Using Energetic Electron Beams And Active Photoemission,” *Spacecraft Charging Technology Conference*, virtual, April 4–8 2022.
- [4] H. Schaub and Z. Sternovsky, “Active Space Debris Charging for Contactless Electrostatic Disposal Maneuvers,” *Advances in Space Research*, Vol. 43, No. 1, 2014, pp. 110–118, dx.doi.org/10.1016/j.asr.2013.10.003.

- [5] M. Bengtson, J. Hughes, and H. Schaub, "Prospects and Challenges for Touchless Sensing of Spacecraft Electrostatic Potential Using Electrons," *IEEE Transactions on Plasma Science*, Vol. 47, Aug. 2019, pp. 3673–3681, 10.1109/TPS.2019.2912057.
- [6] J. Hammerl and H. Schaub, "Effects of Electric Potential Uncertainty on Electrostatic Tractor Relative Motion Control Equilibria," *Journal of Spacecraft and Rockets*, Vol. 59, March – April 2022, pp. 552–562, 10.2514/1.A35165.
- [7] K. Wilson and H. Schaub, "X-Ray Spectroscopy for Electrostatic Potential and Material Determination of Space Objects," *IEEE Transactions on Plasma Science*, Vol. 47, Aug. 2019, pp. 3858–3866, 10.1109/TPS.2019.2910576.
- [8] S. Ranvier, M. Anciaux, P. Cardoen, E. Gamby, I. S. Bonnewijn, J. De Keyser, D. Pieroux, and J. P. Lebreton, "Use of a Langmuir Probe Instrument on Board a Pico-Satellite," *IEEE Transactions on Plasma Science*, Vol. 45, No. 8, 2017, pp. 2007–2012, 10.1109/TPS.2017.2700211.
- [9] K. T. Wilson, M. T. Bengtson, and H. Schaub, "X-ray Spectroscopic Determination of Electrostatic Potential and Material Composition for Spacecraft: Experimental Results," *Space Weather*, Vol. 18, Apr. 2020, pp. 1–10, 10.1029/2019SW002342.
- [10] M. T. Bengtson, K. T. Wilson, and H. Schaub, "Experimental Results of Electron Method for Remote Spacecraft Charge Sensing," *Space Weather*, Vol. 18, Mar. 2020, 10.1029/2019SW002341.
- [11] K. Wilson, Á. Romero-Calvo, M. Bengtson, J. Hammerl, J. Maxwell, and H. Schaub, "Development and characterization of the ECLIPS space environments simulation facility," *Acta Astronautica*, Vol. 194, May 2022, pp. 48–58, 10.1016/j.actaastro.2021.12.037.
- [12] S. T. Lai, *Fundamentals of Spacecraft Charging*. Princeton University Press, Oct. 2011, 10.2307/j.ctvc4j2n.
- [13] R. Hippler, S. Pfau, M. Schmidt, and K. H. Schoenbach, *Low temperature plasma physics: fundamental aspects and applications*. 2001.
- [14] P. Lundgreen and J. Dennison, "Strategies for Determining Electron Yield Material Parameters for Spacecraft Charge Modeling," *Space Weather*, Vol. 18, No. 4, 2020, <https://doi.org/10.1029/2019SW002346>.
- [15] B. Draine and E. Salpeter, "On the physics of dust grains in hot gas," *The Astrophysical Journal*, Vol. 231, 1979, pp. 77–94.
- [16] P. Lundgreen, "The Development and Use of a Secondary Electron Yield Database for Spacecraft Charge Modeling," 2020.
- [17] V. Hariharan, S. Shastry, A. Chakraborty, and V. Katti, "Development of circuit model for spacecraft charging studies," *Proceedings of the International Conference on Electromagnetic Interference and Compatibility*, 1999, pp. 83–90, 10.1109/ICEMIC.1999.871604.
- [18] M. Bengtson and H. Schaub, "Electron-Based Touchless Potential Sensing of Shape Primitives and Differentially-Charged Spacecraft," *AIAA Journal of Spacecraft and Rockets*, Vol. 58, Nov. – Dec. 2021, pp. 1847–1857, 10.2514/1.A35086.
- [19] A. Romero Calvo, J. Hammerl, and H. Schaub, "Touchless Potential Sensing of Differentially Charged Spacecraft Using Secondary Electrons," *Journal of Spacecraft and Rockets*, Vol. 59, No. 3, 2022, pp. 739–750, 10.2514/1.A35355.
- [20] J. E. Borovsky and G. L. Delzanno, "Do Impulsive Solar-Energetic-Electron (SEE) Events Drive High-Voltage Charging Events on the Nightside of the Moon?," *Frontiers in Astronomy and Space Sciences*, Vol. 8, 5 2021, 10.3389/fspas.2021.655333.
- [21] J. Guo, D. Wang, Y. Xu, X. Zhu, K. Wen, G. Miao, W. Cao, J. Si, M. Lu, and H. Guo, "Secondary electron emission characteristics of Al₂O₃ coatings prepared by atomic layer deposition," *AIP Advances*, Vol. 9, No. 9, 2019, p. 095303, 10.1063/1.5113671.